LAPPEENRANTA UNIVERSITY OF TECHNOLOGY
School of Technology
Technomathematics and Technical Physics (Technical Physics)

Igors Krainukovs

NEGATIVE REFRACTIVE INDEX MATERIALS AND PROPAGATION

Examiners: Ph.D. / Associate professor Erik Vartiainen
Ph.D. / Professor Tuure Tuuva

ABSTRACT

Lappeenranta University of Technology
School of Technology
Technomathematics and Technical Physics (Technical Physics)

Igors Krainukovs

Negative Refractive Index Materials and Propagation

Master's thesis

2014

47 pages, 40 figures

Examiners: Ph.D. / Associate professor Erik Vartiainen
Ph.D. / Professor Tuure Tuuva

Keywords: negative refractive index, metamaterials, left-handed materials, dielectric permittivity, magnetic permeability, the Snell's law, diffraction limit, the perfect lens

Negative refractive index materials and propagation of electromagnetic waves in them started to draw attention of scientists not so long ago. This review highlights historically important and recent papers on practical and theoretical aspects related to these issues. Namely, basic properties and peculiarities of such materials related to both their design and wave propagation in them, experimental verification of predictions theoretically made for them, possible practical applications and prospects in this area are considered.

ACKNOWLEDGEMENTS

The author expresses hereby his gratitude to his supervisor professor Erik Vartianen, the second examiner professor Tuure Tuuva, all other people who will read this review (if any), Lappeenranta University of Technology for the excellent educational environment, the Finnish state for the financial support the author has been enjoying during his study at LUT, as well as all those who contributed to the author's knowledge in the realm of physics in the previous years.

Igors Krainukovs

May 14, 2014

TABLE OF CONTENTS

LIST OF ABBREVIATIONS

NRI	-	Negative Refractive Index
LHM	-	Left-Handed Material
RHM	-	Right-Handed Material
DNM	-	Double-Negative Material
TM	-	Transverse Magnetic
TE	-	Transverse Electric

1 INTRODUCTION

1.1 Structure of the thesis

The present review highlights the history of the development in the area of negative refractive index materials and wave propagation in them. In particular, the most important properties of such materials related to wave propagation, their modeling, design and practical realization, experiments carried out with them, possible applications of them as well as prospects in this area are considered.

Introduction is mainly devoted to the special features of propagation of electromagnetic waves in a material with negative refractive index. Chapter 2 highlights the issues related to composition and design of such materials. Chapter 3 describes experiments with such materials which confirmed the special properties of the materials in question. Chapter 4 is fully devoted to theoretical and practical aspects related to the so called perfect lens. Lastly, Chapter 5 summarizes the review.

1.2 Major features of wave propagation in materials with negative refractive index

Although some aspects typical for negative refractive index (further "NRI") materials were discussed in works dated as of the first half of the 20th century (for example, see the reference list in [2]), a systematic research in the area of NRI-materials does not seem to have started until article [1] by a Soviet physicist Victor Veselago was published in Russian in 1967. The paper thus became the pioneering work in the area of NRI-materials. It is mentioned virtually in every paper related to this topic, and then usually with number 1 in the reference list.

In his "What if?"-type article [1], Veselago considered a material with simultaneously negative values of its dielectric permittivity ε and magnetic permeability μ, and especially emphasized that such materials had not been observed by that time. He namely pointed out that, assuming the loss-free isotropic case, such situation is not formally "forbidden", because simultaneous negativity of these two values does not affect the well-known expressions for dispersion

$$k^2 = \frac{\omega^2}{c^2} n^2 \tag{1.1}$$

and refractive index

$$n^2 = \varepsilon\mu. \tag{1.2}$$

Further, he showed that from the Maxwell equations, which in case of a plane monochromatic wave look like

$$[\boldsymbol{kE}] = \frac{\omega}{c}\mu\boldsymbol{H}, \tag{1.3a}$$

$$[\boldsymbol{kH}] = -\frac{\omega}{c}\varepsilon\boldsymbol{E}, \tag{1.3b}$$

it follows that the vectors $\boldsymbol{E}$, $\boldsymbol{H}$ and $\boldsymbol{k}$ form a left-handed triplet of vectors when $\varepsilon < 0$ and $\mu < 0$, as opposite to a more common case of positive ε and μ when these vectors are a right-handed set. This is why materials with $\varepsilon < 0$ and $\mu < 0$ are often called left-handed materials (further "LHM"), whereas more common materials are called right-handed materials (further "RHM"). On the other hand, the Poynting vector

$$\boldsymbol{S} = \frac{c}{4\pi}[\boldsymbol{EH}] \qquad (1.4)$$

does not depend on either ε or μ, and therefore $\boldsymbol{E}$, $\boldsymbol{H}$ and $\boldsymbol{S}$ always form a right-handed set of vectors. An important conclusion which can be immediately drawn is that the wave vector and the Poynting vector (and, consequently, group and phase velocity) are antiparallel to each other in a LHM (whereas in a RHM, these two vectors are co-parallel). This circumstance changes many propagation-related properties in the "reverse" way as compared to a RHM. This is true, for example, for the Vavilov-Cherenkov radiation (the radiation cone in a LHM is directed backward relative to the velocity of a charged particle) and the Doppler effect. Namely, presuming the velocity of a detector and the phase velocity of the wave detected being collinear, the detected frequency ω is related to the radiated frequency ω_0 in the following way:

$$\omega = \omega_0\left(1 - p\frac{v}{u}\right), \qquad (1.5)$$

where p = +1 for a RHM, p = -1 for a LHM, v is the velocity of the detector ($v > 0$ if the detector moves from the source), u is the velocity of the energy flux (u is always positive). According to (1.5), if the detector is approaching the source in a LHM, the detected frequency ω is smaller than the emitted frequency ω_0, whereas in a RHM ω would exceed ω_0.

Veselago argues further that the well-known boundary conditions for the components of magnetic and electric field at the interface between two media shall hold independently of whether the media are left- or right-handed. This ultimately means that in the case when the media in question have different rightness, the ray refracted will propagate on the same side relative to the interface normal as the incident ray, whereas the propagation direction of the ray reflected is not affected by which rightness the media have.

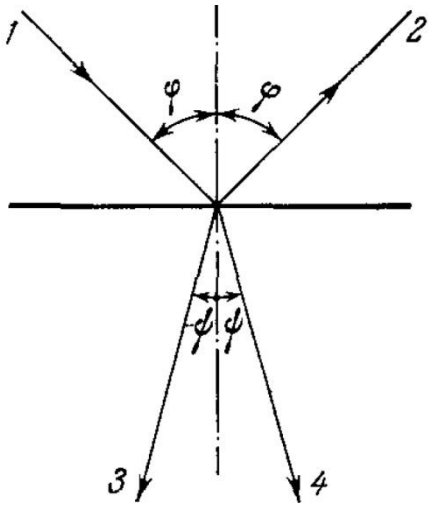

Figure 1.1 [1]. Refraction and reflection when the two media have the same and different rightness. 1 – incident ray, 2 – reflected ray, 3 - refracted ray if the lower medium is left-handed (the refraction angle is negative in this case), 4 - refracted ray if the lower medium is right-handed. The upper medium is presumed to be right-handed

Hence, the Snell's law should be rewritten in a more general form, namely

$$\frac{\sin\varphi}{\sin\psi} = n_{1,2} = \frac{p_2}{p_1}\left|\sqrt{\frac{\varepsilon_2\mu_2}{\varepsilon_1\varepsilon_1}}\right|, \qquad (1.6)$$

where p_i is the rightness of the respective medium (i = 1 corresponds to the upper medium). This particularly means that the absolute refractive index of a LHM is negative. It should be noted that the choice of the minus sign for the refractive index of a LHM represented as $(\mu\varepsilon)^{½}$ is hardly obvious and ultimately follows from the causality principle (see, for example, [3]).

Veselago predicts also unavoidable dependence of both ε and μ on frequency ω for the case of a LHM. This is because otherwise the expression for electromagnetic field energy density

$$W = \frac{\partial(\varepsilon\omega)}{\partial\omega}E^2 + \frac{\partial(\mu\omega)}{\partial\omega}H^2 \qquad (1.7)$$

would reduce to $W = \varepsilon E^2 + \mu H^2$ yielding a non-physical negative value for W if $\varepsilon < 0$ and $\mu < 0$. Evidently, the both derivatives in (1.7) must be positive.
Some other ideas mentioned in [1] are presented in Chapters 2 and 4 of the present review.

In conclusion of this Chapter, the following should be mentioned. One may think that it is enough to change the sign of the refractive index to make an expression related to electromagnetic wave propagation correct also in the case of a NRI-material. But this is true only partially, and one has to be cautious doing so. This is because many expressions are often written for a non-magnetic medium which have μ equal to 1. Hence, as this is mentioned in [4], one should first rewrite an expression in the most general way for a RHM and only then make transition to the case of a LHM. This implies that some expressions (for example, those analytically representing the Snell's law, the Cherenkov radiation and the Doppler effect), indeed, are rewritten by means of a plain substitution of n by $-n$. Some other relations, however, should be first written in the form where the information on the electromagnetic properties of a medium is presented by either impedance $z = (\mu/\varepsilon)^{1/2}$, which, unlike the refractive index, does not change its sign in a LHM (for instance, when modifying the Fresnel equations), or explicitly by ε and μ (for example, when modifying the expression for the Brewster's angle) rather than the refractive index.

An interesting (and not obvious) example of a fundamental fact which also holds for a LHM is the Kramers-Kronig relations. In [12], a rather general single resonance Lorentzian model for both complex permittivity and complex permeability is considered. In other words, these values are presented as frequency dependent functions in the following way:

$$x(\omega) = 1 + \frac{\omega_{pq}^2}{\omega_{0q}^2 - \omega^2 - i\gamma_q\omega}, \qquad (1.8)$$

where q is either e or m depending on whether $x(\omega)$ is $\varepsilon(\omega)$ or $\mu(\omega)$. Provided $\omega^2_{pq} > \gamma^2_q + 2\gamma_q\omega_{0q}$, the real part of the corresponding value is negative, meaning that the both real parts might be simultaneously negative in an overlapping frequency

range, which in its turn implies that the medium has negative values of the real part of its complex refractive index $N(\omega)$ in this overlapping frequency range as shown in Fig. 1.2.

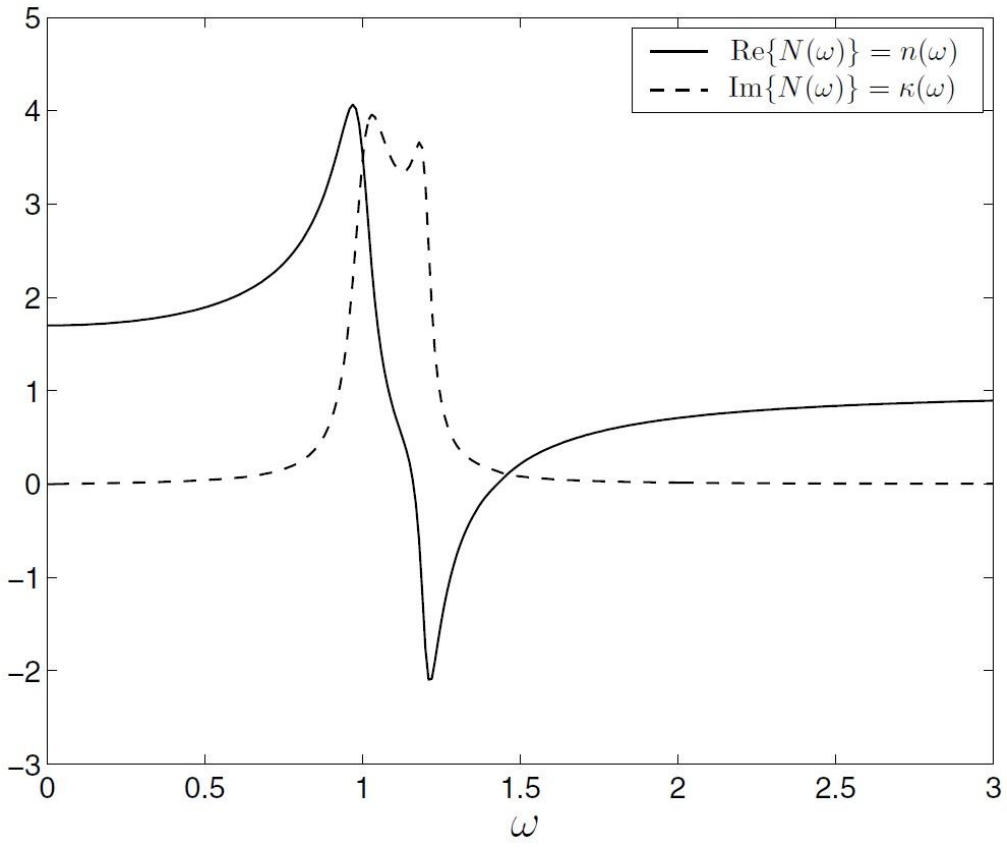

Figure 1.2 [12]. The real part of the refractive index may change its sign within the framework of the single resonance Lorentzian model for complex ε and μ. Here $\omega_{0e} = 1$, $\omega_{pe} = 1$, $\gamma_e = 0.1$, $\omega_{0m} = 1.2$, $\omega_{pm} = 0.8$, $\gamma_m = 0.05$

On the other hand, the authors restore the real and the imaginary part of the refractive index $N(\omega')$ applying the Kramers-Kronig relations:

$$\mathrm{Re}(N(\omega')) \equiv n(\omega') = 1 + \frac{2}{\pi} P \int_0^{\infty} \frac{\omega k(\omega)}{\omega^2 - \omega'^2} d\omega, \qquad (1.9\ \text{a})$$

$$\mathrm{Im}(N(\omega')) \equiv k(\omega') = -\frac{2\omega'}{\pi} P \int_0^{\infty} \frac{n(\omega) - 1}{\omega^2 - \omega'^2} d\omega. \qquad (1.9\ \text{b})$$

The values obtained as the result of the calculations according to the Kramers-Kronig relations, n_{KK} and k_{KK}, are then compared to respectively n_{true} and k_{true} (which are the values calculated directly from (1.8)) in a rather wide frequency range including the band where n_{true} is negative. The comparison indicates coincidence of the values "within the precision of the numerical integration" throughout the whole frequency region considered, implying the Kramers-Kronig relations are valid also in the case of a negative real part of refractive index.

2 COMPOSITION OF LEFT-HANDED MATERIALS

Despite the intriguing properties of the LHM described in [1], the topic had been more or less neglected during about 30 years, most probably due to lack of such materials. Their design turned out to be a rather difficult task which, actually, was more or less predicted in [1], where Veselago, in addition to description of properties of an abstract LHM, gave also some hints on how materials of this type might be composed practically. Namely, he first took up the isotropic case and remembered that in plasma, at relatively low frequencies, the dielectric permittivity is negative.

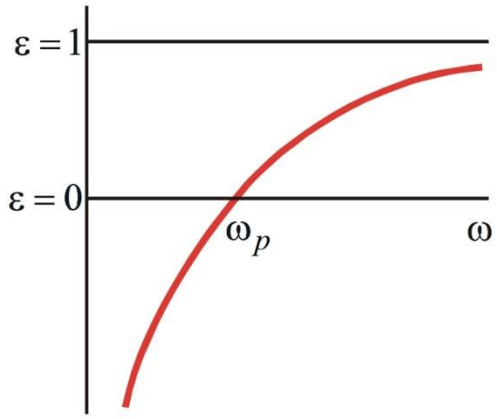

Figure 2.1 [3]. A qualitative representation of the typical dependence of the real part of the permittivity of a plasma on frequency. Below the plasma frequency, this value is negative

On the other hand, as Veselago mentioned, there is no known isotropic substance which would have $\mu < 0$. This ultimately true due to the fundamental fact that "the sources of magnetic field are not charges but dipoles". In other words, one cannot simply mix an ordinary plasma with a gas of magnetic monopoles, making a mixture which would be left-handed in the frequency range where both ε and μ are negative, just because there are no such monopoles. However, Veselago mentioned that anisotropic LHMs are quite feasible and are to be looked for "primarily among gyrotropic media" where both ε and μ are tensors, for example, among pure

ferromagnetic metals. The refractive index for a plane circularly polarized wave propagating along the external magnetic field in such a medium can be expressed in terms of ε and μ in the following way:

$$n^2 = (\varepsilon_1 \pm \varepsilon_2)(\mu_1 \pm \mu_2), \qquad (2.1)$$

which means that the wave corresponding to the both factors in this expression being negative is quite possible. The drawback of such a proposal is obvious: a negative refractive index can be true only for the waves propagating at a very small angle between their wave vector and the external magnetic field.

This Veselago's recipe, however, has not been to become of a greater value for the progress in design of LHMs. In his much later article [4], he admits: "We have put a lot of efforts into designing a negative refractive index material based on $CdCr_2Se_4$ magnetic semiconductor. These efforts, however, have not been rewarded due to significant technological problems related to synthesis of this material". As we will see, the unusual features of the modern metamaterials* owe to their special structure rather than the chemical or magnetic properties of their constituents. A great contribution to this kind of development in the metamaterial design was made by sir John Pendry.

In paper [5] from 1996, Pendry et al. describe dispersive properties of a periodic structure composed of infinitely long thin wires arranged in a simple cubic lattice as it is shown below.

---

* Here and further in the present review, materials with the real part of μ and/or ε being negative might be mentioned as metamaterials

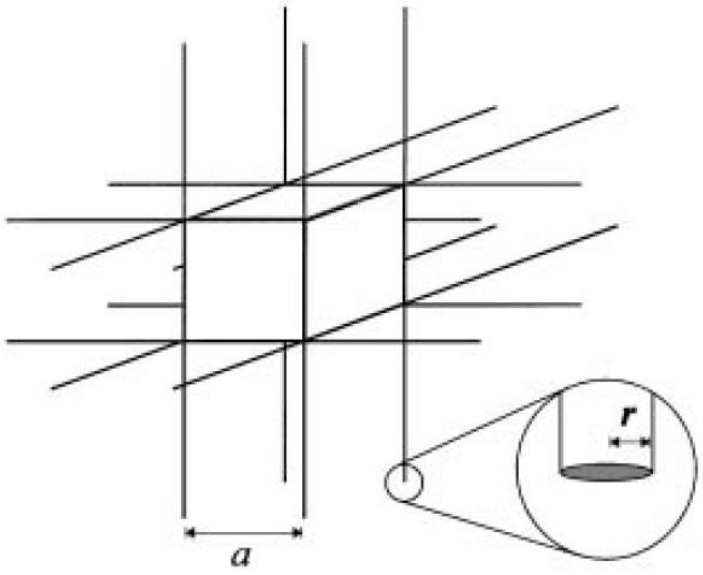

Figure 2.2 [5]. The periodic structure composed of thin wires mimicking the dielectric response of a plasma

The plasma frequency of such a structure, given by the well-known expression

$$\omega_p^2 = \frac{n_{eff}e^2}{\varepsilon_0 m_{eff}}, \tag{2.2}$$

is shifted to much lower frequencies as compared to a pure metal constituting the wires. This is mainly due to the self-inductance of the wire structure as it enhances the effective mass so, that the electrons "are as heavy as nitrogen atoms", whereas the effective concentration gets lower than the electron concentration in the metal. This is because the both effective values heavily depend on the lattice geometry, and so does the plasma frequency:

$$\omega_p^2 = \frac{2\pi c_0^2}{a^2 \ln(a/r)}. \tag{2.3}$$

Presuming some feasible values for *a* and *r* and that the wires are made of aluminium, the plasma frequency of the structure has a value of approximately 10 GHz which is to be compared with the plasma frequency of pure Al lying in the UV range. From the viewpoint of metamaterial design, however, the most important here is not this decrease in ω_p, but the very fact that the plasma-like response can be given by a

rather simple and lightweight structure having the complex effective permeability as follows:

$$\varepsilon_{\text{eff}} = 1 - \frac{\omega_{\text{p}}^2}{\omega(\omega + i\varepsilon_0 a^2 \omega_{\text{p}}^2/\pi r^2 \sigma)}, \tag{2.4}$$

where σ is the conductivity of the metal.

However, such thin wire structures were not anything new and, according to, for example, [7], were in particular used to study microwave propagation through the ionosphere already in the middle of the last century.

Pendry's great contribution to metamaterial design lies in his investigation of structures made of non-magnetic metal but giving a magnetic response, including negative permeability at some frequency range, presented in [6]. In this paper, Pendry et al. consider some periodical metallic structures and analyze their effective permeability $\mu_{\text{eff}} = B_{\text{ave}}/\mu_0 H_{\text{ave}}$, where the averaging is carried out over the unit cell of a periodic structure (see below).

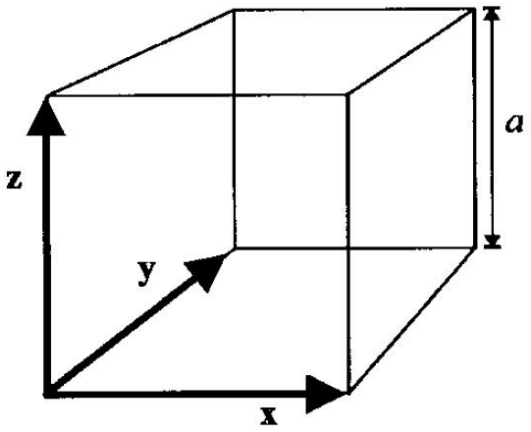

Figure 2.3 [6]**.** The unit cell of the periodic structure

The authors start with an anisotropic structure formed by metallic cylinders as shown in Fig. 2.4.

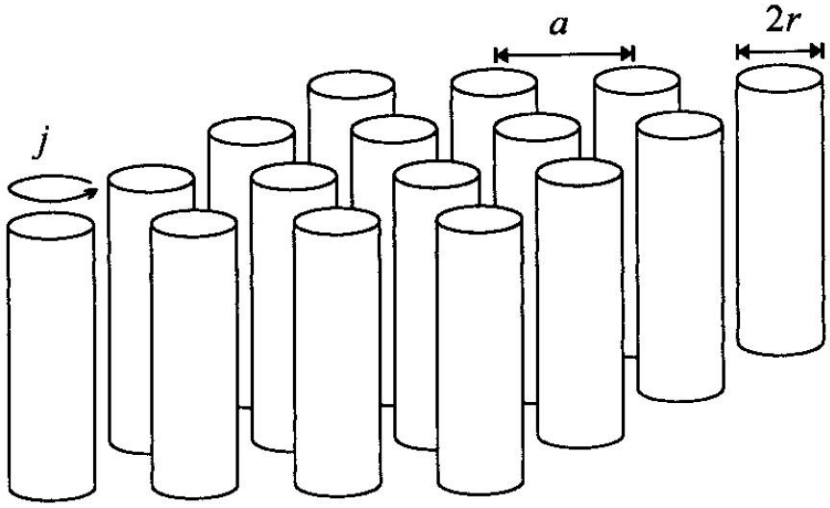

Figure 2.4 [6]. A periodic structure constituted by metallic cylinders

Presuming that the external magnetic field is parallel to the axes of the cylinders, the structure has a frequency dependent μ_{eff} which is governed by the unit cell size a, the cylinder radius r and the resistivity of the metal used. Presuming the cylinders are thin ($r << a$), the real part of μ_{eff} is always less than 1 and higher than 0.

The next step is introduction of capacitance into the system by substituting the solid cylinders with two separated metal sheets as shown in Fig. 2.5.

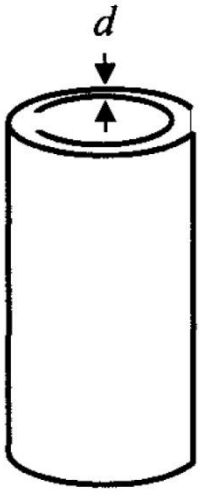

Figure 2.5 [6]. The endlessly long two-sheet cylindrical structure

Thanks to the capacitance, the external magnetic field now enables current to flow as shown in Fig. 2.6.

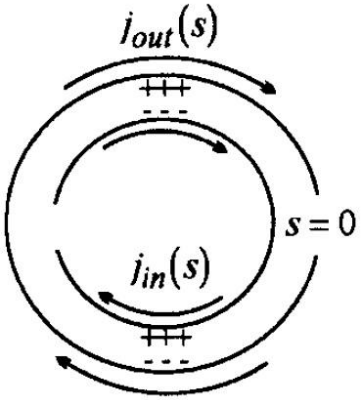

Figure 2.6 [6]. The capacitance of the structure enables the external magnetic field parallel to its axis to induce current in it

Above the resonance frequency ω_0, the permeability of the structure in question has qualitatively the same frequency dependence as the permittivity of a typical non-lossy plasma (see Fig. 2.7).

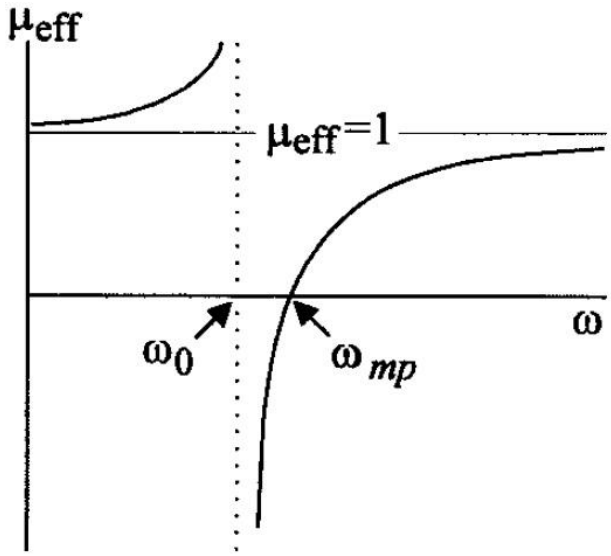

Figure 2.7 [6]. The effective permeability of an array of the two-sheet cylinders. The material is presumed to be highly conductive

The most interesting here is the region between ω_0 and the "magnetic plasma frequency" ω_{mp} where the effective permeability is negative. The both frequencies depend solely on the geometrical parameters of the two-sheet cylinder and the lattice constant *a*.

Lastly, the authors substitute the two-sheet cylinders with stacks of thin split rings. The geometry of the rings and their arrangement is shown in Fig. 2.8.

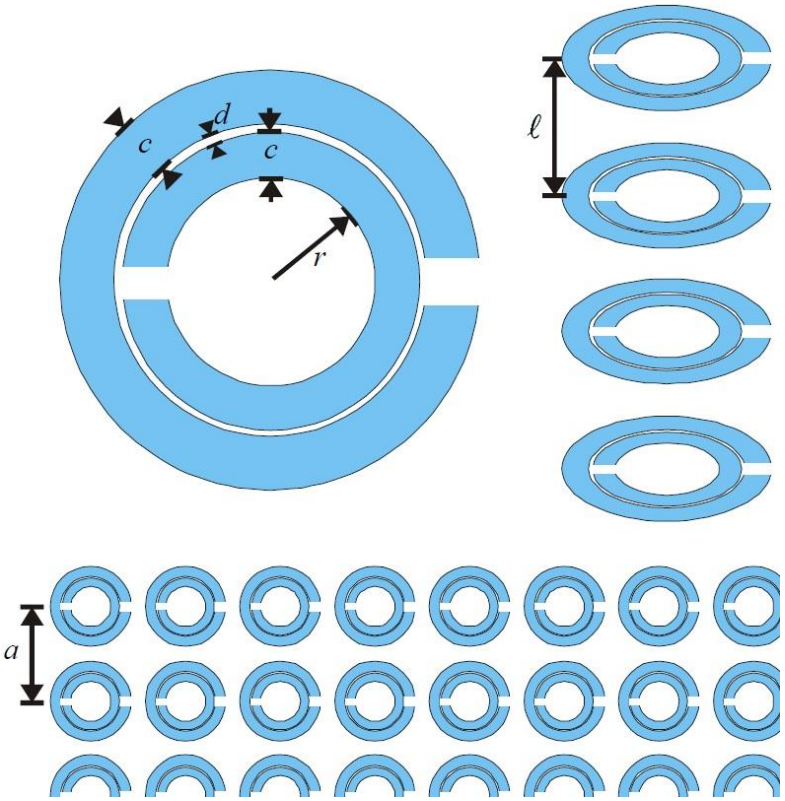

Figure 2.8 [3]. The geometry of the split rings and their arrangement

Presuming $r >> c$, $r >> d$, $l < r$, $\ln(c/d) >> \pi$, the frequency dependence of the effective permeability is expressed through the geometrical and electrical parameters of the system in the following way:

$$\mu_{\text{eff}} = 1 - \frac{\frac{\pi r^2}{a^2}}{1+\frac{2l\sigma i}{\omega r \mu_0} - \frac{3lc_0^2}{\pi\omega^2 \ln\frac{2c}{d} r^3}}, \qquad (2.5)$$

where σ is the resistance of unit length of the sheets composing a ring measured around the circumference. Fig. 2.9 presents an example of this dependence calculated for some typical values of the geometrical parameters and the specific resistance. A frequency range where the real part of μ_{eff} is negative is clearly seen.

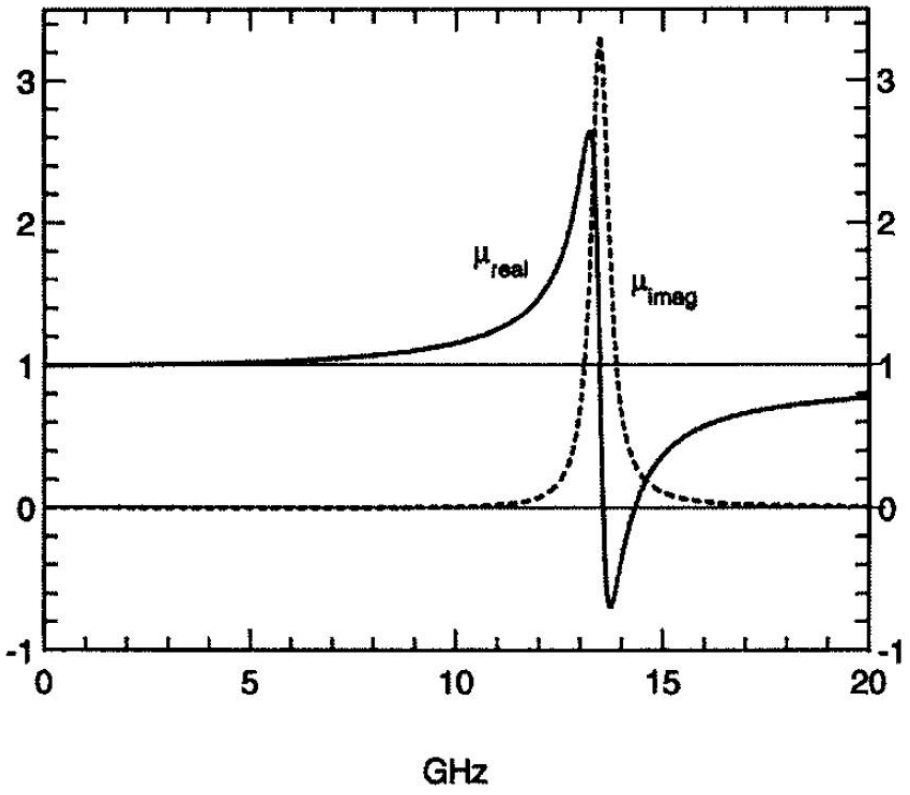

Figure 2.9 [6]. The real and imaginary part of the permeability of the system of stacked rings as functions of frequency. $a = 10^{-2}$ m, $c = 10^{-3}$ m, $d = 10^{-4}$ m, $l = 2*10^{-3}$ m, $r = 2*10^{-3}$ m, $\sigma = 2*10^{3}$ ohm/m

It is important to mention that the split ring structure can be readily used to make an isotropic material with negative μ_{eff} as shown in Fig. 2.10.

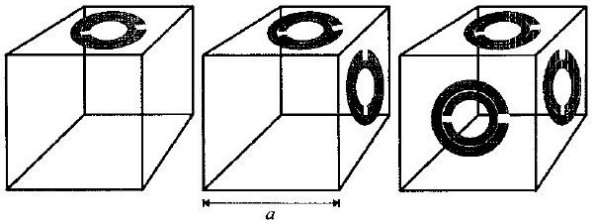

Figure 2.10 [6]. Making a cubic unit cell of an isotropic material with split rings

This idea of Pendry was very soon followed by the proposal of Smith et al. [7] to combine the split ring structure with the thin wire structure to obtain a LHM. They simulated the response of a system of layers of split rings with parallel thin wires of a radius of 0.8 mm placed between the rings. The dispersion dependence for the case when the incident electric field is parallel to the wires and the magnetic field is parallel to the axis of the rings is shown in Fig. 2.11.

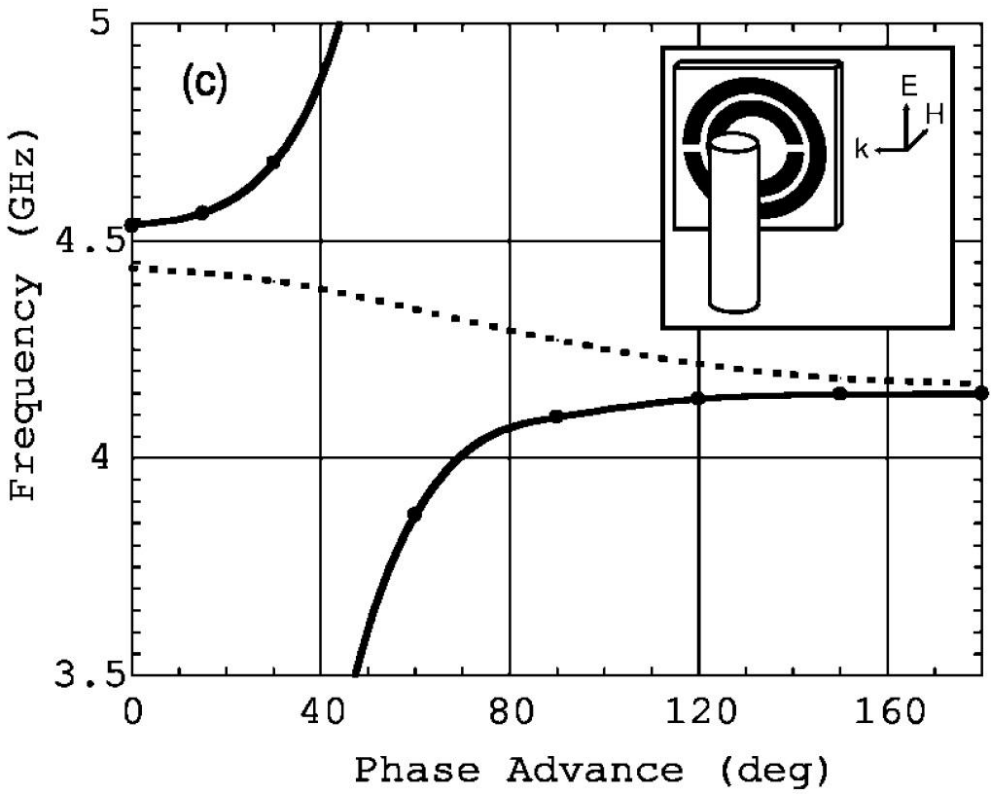

Figure 2.11 [7]. Frequency versus *kd*. Ring parameters: c = 0.8 mm, d = 0.2 mm, r = 1.5 mm; lattice constant a = 8.0 mm

It should be noted that the resonance frequency of a stack of split rings is given by the following expression [6]:

$$\omega_0^2 = \frac{3lc_0^2}{\pi \ln\frac{2c}{d} r^3}. \qquad (2.6)$$

The typical values of the parameters (those considered in Fig. 2.9) yields ω_0 = 13.5 GHz. Obviously, smaller values of the ring radius yields higher resonant frequencies. Shalaev [2] reports that one has managed to push up ω_0 to 1 THz thanks to the scaling technique.

As to higher frequencies including the very important optical frequency range, different structures are used to create LHMs. An important example here is the double periodic array of pairs of parallel gold nanorods [8], a particular realization of which is shown in Fig. 2.12.

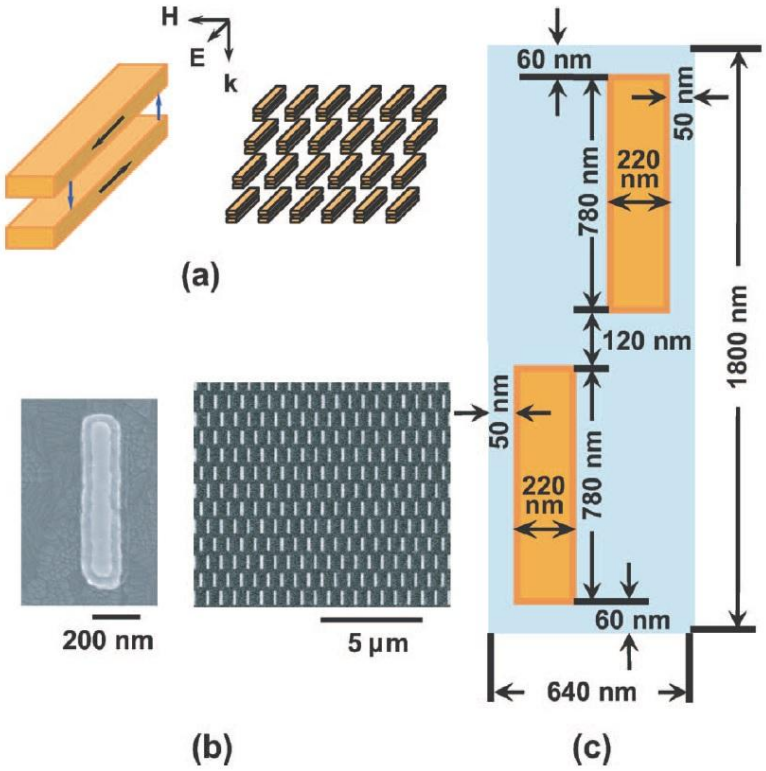

Figure 2.12 [8]. (a)The double periodic array of pairs of parallel gold nanorods and the incident field; (b) FESEM-images of the array of rods and a single rod; (c) geometrical parameters of the elementary cell of the array

The structure may be thought of in terms of an LC-circuit, where the rods provide the inductance and the dielectric gaps between the rods are capacitances. Both the electric and the magnetic responses of the system have resonance behavior, provided the incident electromagnetic wave is polarized as shown in Fig. 2.12, meaning the refractive index may be negative above the resonance frequency. The calculations and the experimental data for the real part of the refractive index of a structure of such a type are shown in Fig. 2.13 indicating that it is negative in the vicinity of a wavelength of about 1.5 μm ($n' = -0.3 \pm 0.1$ at $\lambda \approx 1.5$ μm).

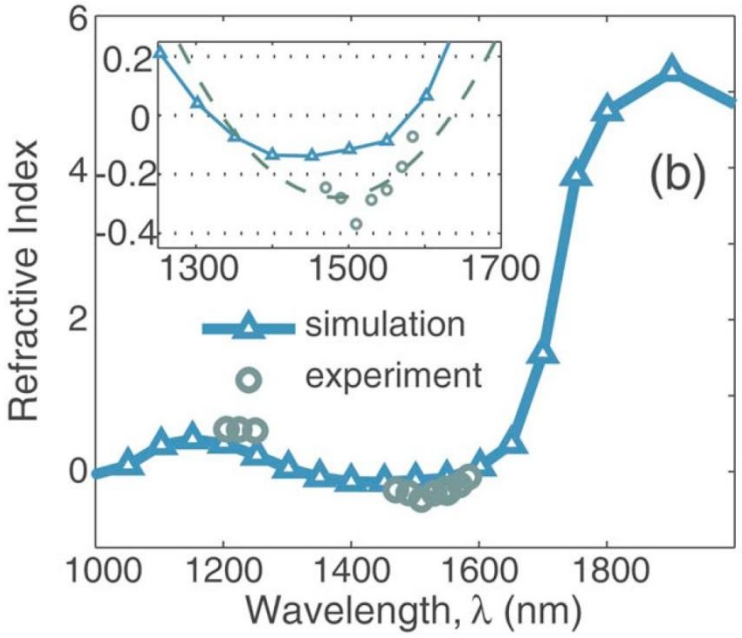

Figure 2.13 [8]. The experiment and simulation results representing the real part of the refractive index of the double-periodic structure described above as a function of wavelength. The real part of the refractive index is negative in the vicinity of a wavelength of 1500 nm

In conclusion of this Chapter, it should be emphasized – as it is emphasized almost in every work related to the topic - that description in terms of some effective permeability, permittivity and refractive index is valid only if “large” values of wavelength are considered. In the case of RHMs, the wavelength shall exceed the

typical size of atoms/molecules of the material, whereas in the case of metamaterials, the wavelength shall exceed the size of the elementary unit cell (for example, the one shown in Fig. 2.10) of the periodic structure. In a sense, such a unit cell acts as a larger "pseudoatom".

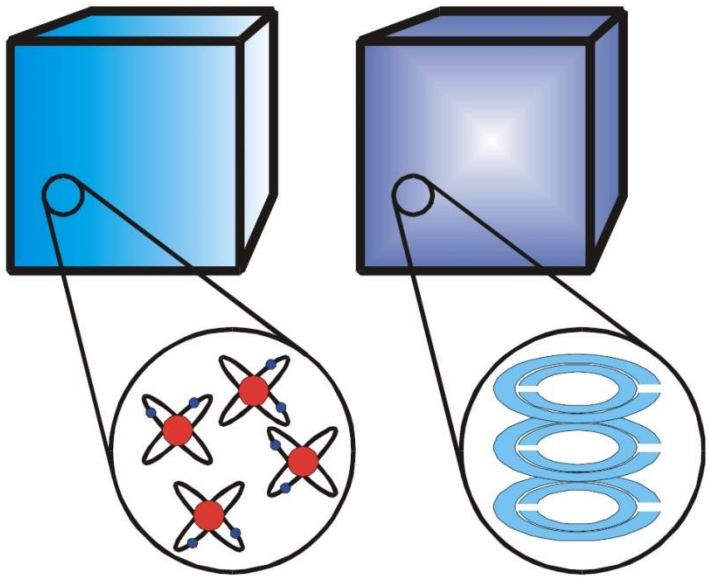

Figure 2.14 [3]. Permittivity and permeability of conventional materials are governed by the properties of their atoms/molecules, whereas those of metamaterials – by the properties of the elementary unit cells which may contain many atoms

3 EXPERIMENTAL VERIFICATION OF UNUSUAL FEATURES OF LEFT-HANDED MATERIALS

3.1 Negative refraction angle

Thanks to the progress in design of metamaterials described in Chapter 2 of the present review, it has become possible to experimentally verify the predictions for LHMs made by Veselago [1]. Checking validity of the Snell's law seems to be the most straightforward and simple way to show that a material investigated is left-handed: if the refraction angle is negative, then the material is really so. Shelby et al. seem to be the first who made such an experiment described in paper [9] from year 2000. They investigated a structure resembling the one modeled in [7]. A photograph of the structure is shown in Fig. 3.1. It was namely a lattice formed by interlocking fiber glass circuit boards. Copper square-shaped split rings and wires were placed on opposite sides of the boards. The lattice unit cell dimension of 5 mm was significantly less than the wavelength of approximately 3 cm corresponding to the frequency of 10.5 GHz of the incident wave used in the experiment. The lattice was expected to have a negative real part of the refractive index in the frequency range from 10.2 GHz to 10.8 GHz.

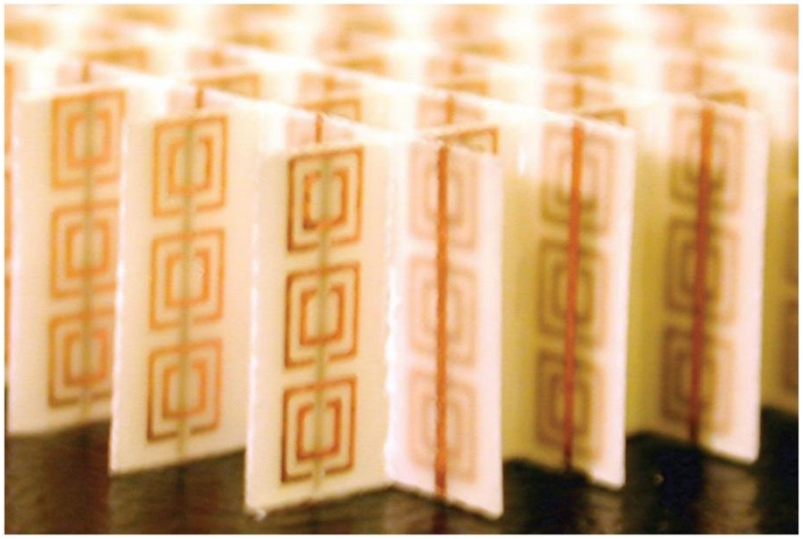

Figure 3.1 [9]. Photograph of the periodic structure investigated in [9]

The experimental setup is schematically shown in Fig. 3.2.

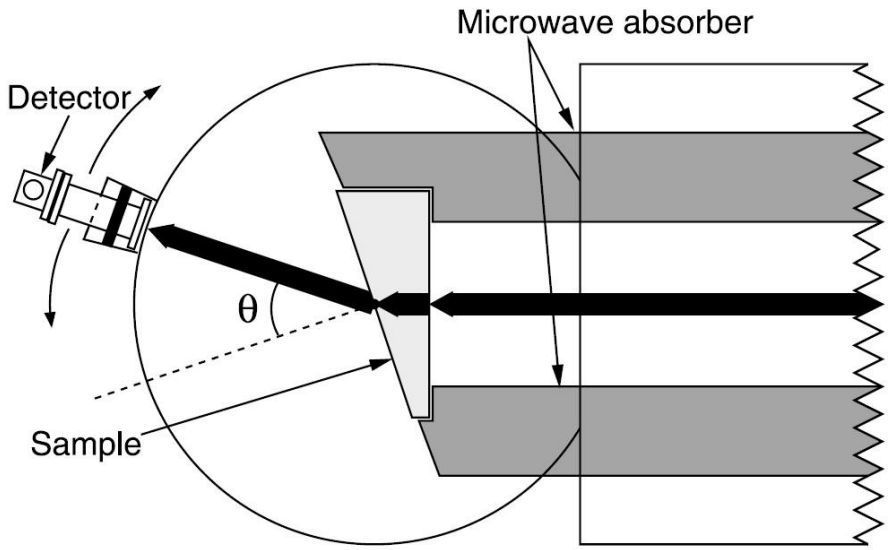

Figure 3.2 [9]. A prism–shaped sample is placed between the circularly shaped metallic plates (shown transparent). A detector rotates around the plates and records the transmitted power spectrum. The thick solid black line depicts the path of the microwave beam if the sample is made of a RHM. The dashed line is the normal to the material-air interface where the beam gets refracted

Prism-shaped pieces of teflon and the LHM described above were investigated. The electric component of the incident field was perpendicular to the image plane and, in the latter case, also parallel to the copper wires. As expected, the peak power transmitted through teflon was detected at a positive angle θ, whereas in the case of the LHM, the refraction angle was measured to be negative, about -61°, indicating that the refractive index was -2.7 ± 0.1.

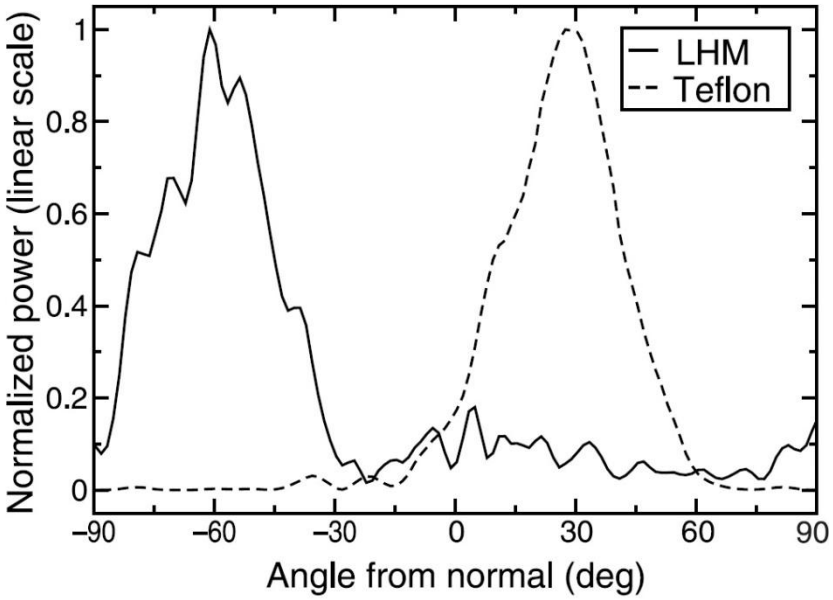

Figure 3.3 [9]. The transmitted power measured versus the presumed refractive angle. The beam width is due to diffraction at the exit of the incident channel and the angular sensitivity of the detector being independent of the properties of the samples investigated

Thus, the validity of the Snell's law for a LHM was successfully demonstrated during the experiment described.

3.2 The reversed Doppler effect

The Doppler effect is also intriguing, especially because it is somewhat unclear how one can carry out a corresponding experiment using, for example, the LHM described above, as a moving source and/or detector would evidently damage the medium. However, such an experiment was carried out (according to the authors, for the first time) with a double negative acoustic medium and described in [10]. A fluid within the tube shown in Fig. 3.4 acquires a negative modulus thanks to the side holes and a negative density thanks to the membranes thus becoming a Double-Negative Medium (DNM).

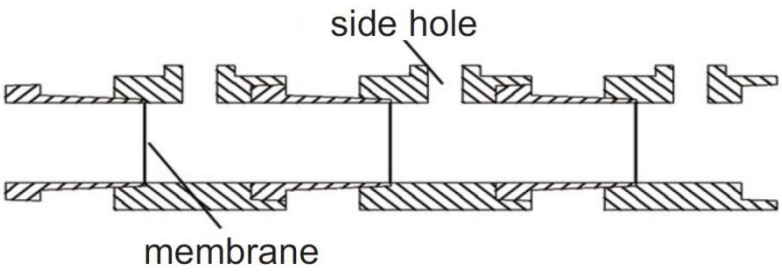

Figure 3.4 [10]. The structure making a fluid within it double-negative

Theoretical predictions for such a medium in a form of dispersion curves are presented in Fig. 3.5.

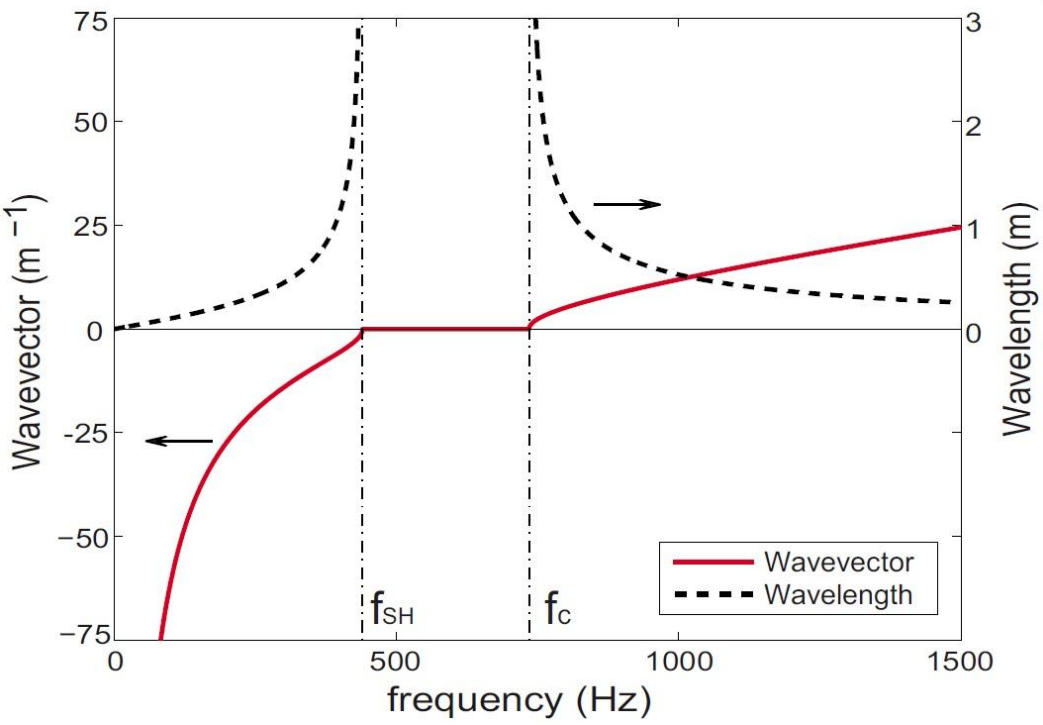

Figure 3.5 [10]. The wavenumber and wavelength of the medium described above versus frequency. The medium is double-negative below f_{SH} and double-positive above f_C. The gap between these cut-off frequencies corresponds to evanescent waves

Actually, the problem with a moving source and/or detector is quite topical also in this case, but the authors suggest the experimental setup schematically shown below arguing that it is equivalent to the situation when the moving source is located within the medium as long as the unit-cell size is much smaller than the wavelength.

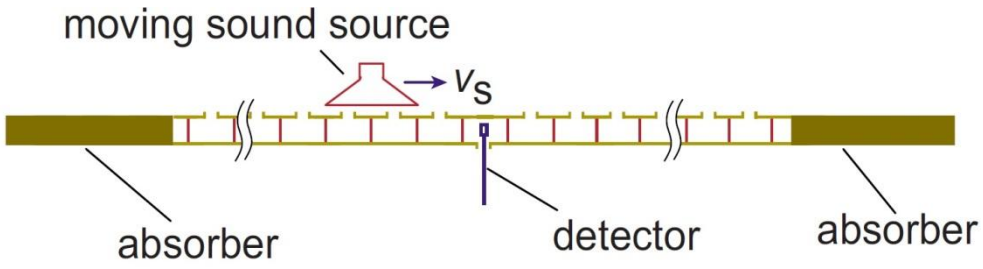

Figure 3.6 [10]. The experimental setup for the verification of the reversed Doppler effect

The frequency shift versus frequency in the case of an approaching source was both measured and calculated according to the following formula:

$$\Delta\omega = s\frac{v_S}{v_0}\omega\sqrt{(1-\omega_{SH}^2/\omega^2)(1-\omega_C^2/\omega^2)}, \qquad (3.1)$$

where s = +1 for a double-positive medium, s = -1 for a double-negative medium, v_S = 5 m/s is the source velocity, sound frequency f = 350 Hz, $v_0 \approx$ 320 m/s is the sound speed in the material in the high frequency limit. The results of the measurements and the calculations are shown in Fig. 3.7.

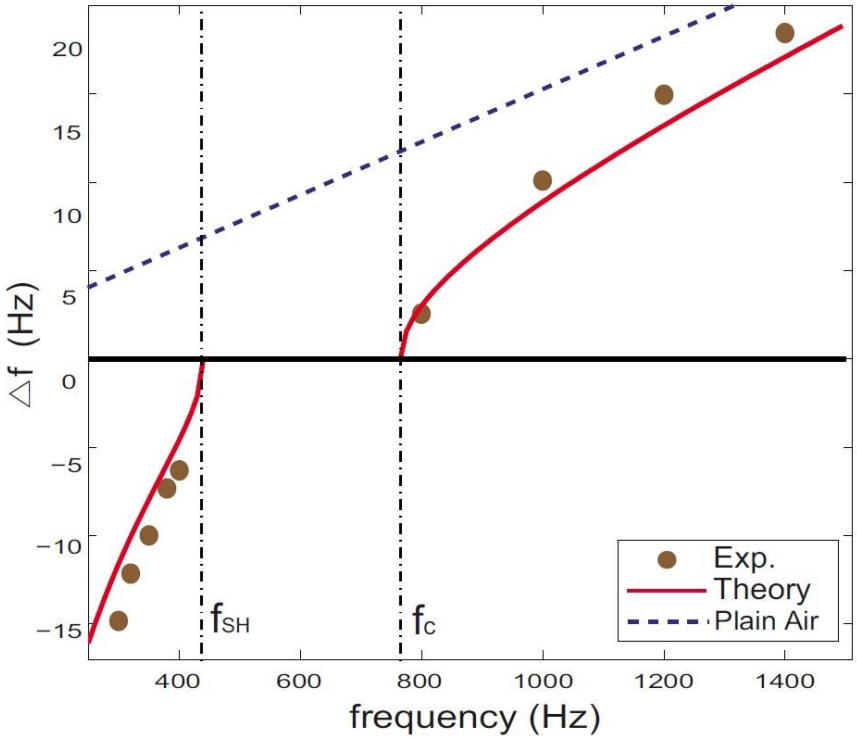

Figure 3.7 [10]. The measured and calculated Doppler shift

As it follows from the figure, in the frequency range where the material behaves as a DNM (that is, below f_{SH}), the shift is negative. The authors emphasize though that the wavelength change in double-positive and double-negative materials is the same, namely, the wavelength in front of a moving source is always shorter than behind it. In other words, the Doppler effect for any double-negative medium is reversed in the frequency domain, whereas in terms of wavelength it remains the same as for more common media.

4 THE PERFECT LENS

In his article [1], Veselago also predicts the ray path through lenses made of a LHM. These predictions follow from the Snell's law and mean that a concave lens made of such a material qualitatively behaves as a convex lens and vice versa.

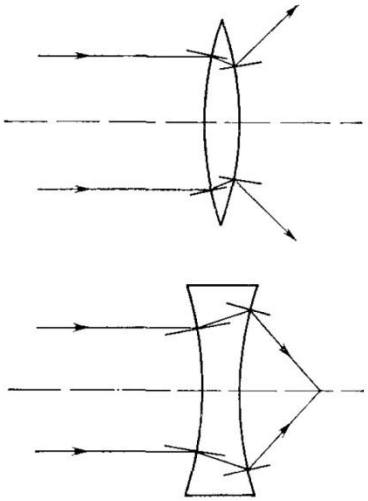

Figure 4.1 [1]. Lenses made of a LHM focus light rays in a "reversed" manner as compared to conventional materials

What might seem even more intriguing, is that a plain slab of a LHM behaves like a focusing lens. The difference from a lens is that the source must be located quite close to the slab rather than be far from it. A ray path through a LHM-slab with $\mu = \varepsilon = -1$placed in free space is shown in Fig. 4.2. Thanks to impedance matching, the light experiences no reflection.

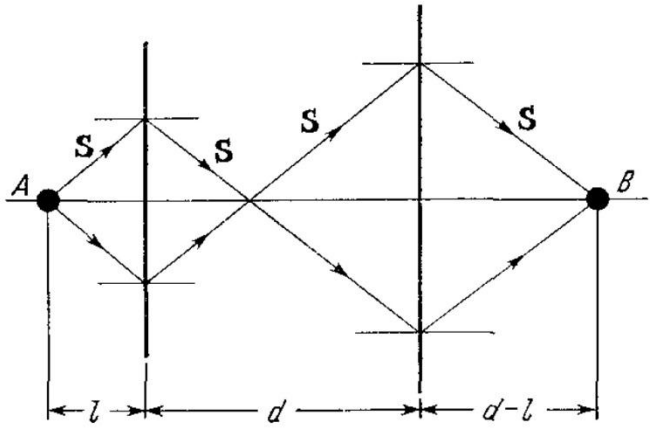

Figure 4.2 [1]. Light propagating through a LHM-slab gets focused twice: once within the slab and then out of the boundaries of the slab (point B).

The question here might be how sharp the second focus is. As it is widely known and shown in Pendry's article [11] published more than 30 years after the paper of Veselago [1], the maximum resolution of the image given by a lens cannot exceed the illumination wavelength λ. Indeed, presuming that the z-axis coincides with the lens axis, the frequency ω and the components of the wavevector $\boldsymbol{k}$ are related to each other in the following way:

$$k_z = \sqrt{\frac{\omega^2}{c^2} - k_x^2 - k_y^2} > 0. \qquad (4.1)$$

If the transverse components of $\boldsymbol{k}$ are small enough, k_z is positive. Otherwise, if $\omega^2 c^{-2} < k_x^2 + k_y^2$, then

$$k_z = i\sqrt{k_x^2 + k_y^2 - \frac{\omega^2}{c^2}}, \qquad (4.2)$$

meaning k_z is imaginary and corresponds to the exponentially decaying evanescent waves. These waves are therefore absent from the image as no lens can restore their amplitude, and this is why the resolution limit mentioned above takes place.

Pendry considers also the behavior of evanescent waves in case when a lens is substituted by the slab with $n < 0$ mentioned in Veselago's paper. He namely takes up both the *p*- and *s*-polarized incident wave and, considering multiple scattering at the boundaries of the slab, shows that, if $n = -1$, the reflection coefficient is 0, whereas transition coefficients for the both cases are given by the following expressions:

$$\lim_{\substack{\mu\to-1\\ \varepsilon\to-1}} T_{\mathrm{S}} = \lim_{\substack{\mu\to-1\\ \varepsilon\to-1}} T_{\mathrm{P}} = \exp\left(-ik_{\mathrm{z}}d\right). \qquad (4.3)$$

Here *d* is the thickness of the slab and *kz* is given by (4.2). It means that the transmission coefficients are positive, and evanescent waves get amplified by the slab. Hence, unlike a common lens, a slab with n = -1 is able to make evanescent waves contribute to formation of the image.

Pendry also presents results of model calculations for a slab made of silver. He takes up a system shown in Fig. 4.3 where all the dimensions are presumed to be significantly smaller than the wavelength. In this case, the electrostatic (for the *p*-polarization) limit is applicable, and the value of permeability – and silver has a positive one - does not play any role.

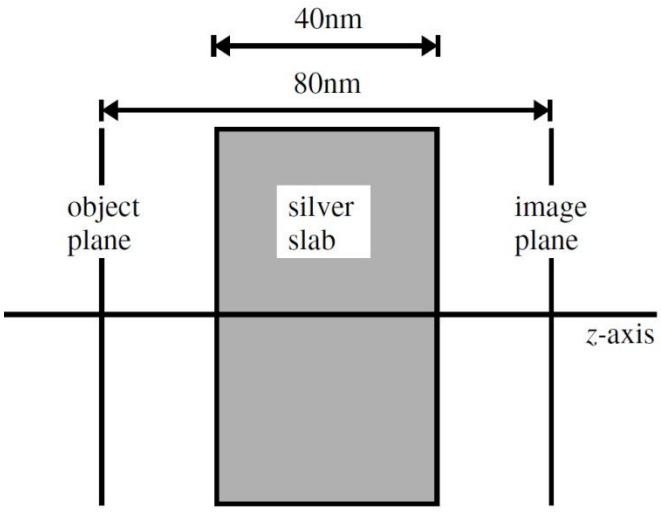

Figure 4.3 [11]. A slab is presumed to be made of silver in order to model the amplification of evanescent waves in the electrostatic limit

The dielectric permittivity of silver is modeled as

$$\varepsilon \approx 5.7 - 81\frac{1}{(\hbar\omega)^2} + 0.4i, \qquad (4.4)$$

where the value of $\hbar\omega$ should be taken in electronvolts.The frequency ω is chosen such that $\hbar\omega$ = 3.48 eV, meaning Re(ε) ≈ -0.99. A two-spike electrostatic potential shown in Fig. 4.4 is considered as a source.

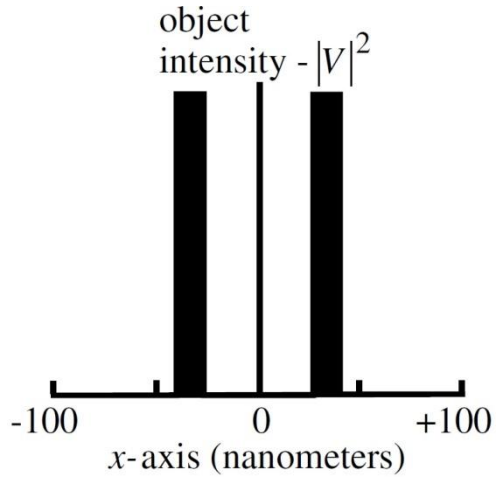

Figure 4.4 [11]. Electrostatic potential considered as a source

The results of calculations for the case when the silver slab is absent and present are shown in the figure below.

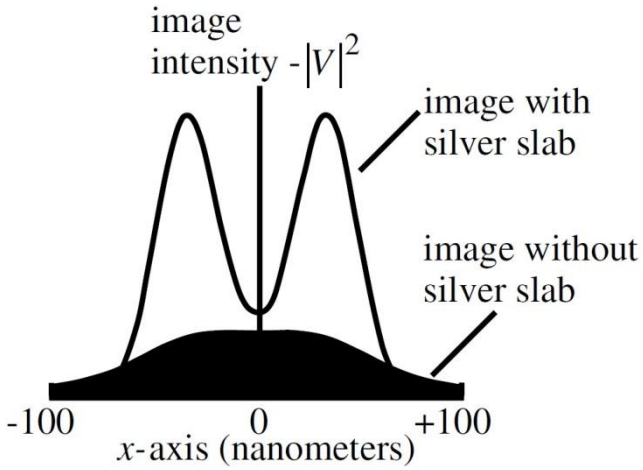

Figure 4.5 [11]. The calculated intensity distribution along the transverse coordinate

Pendry's conclusion is that the silver slab restores the amplitude of the higher order Fourier components of the electrostatic potential, and the only circumstance preventing the lens from being perfect is the non-zero imaginary part of ε.

The case of an "asymmetric lens" where one of the medium surrounding the slab is different from air is more general and might be practically more important as this medium might be solid structure such as glass or GaAs used as a substrate making the system mechanically sturdy. Such a system is shown in Fig. 4.6 and was considered in [13].

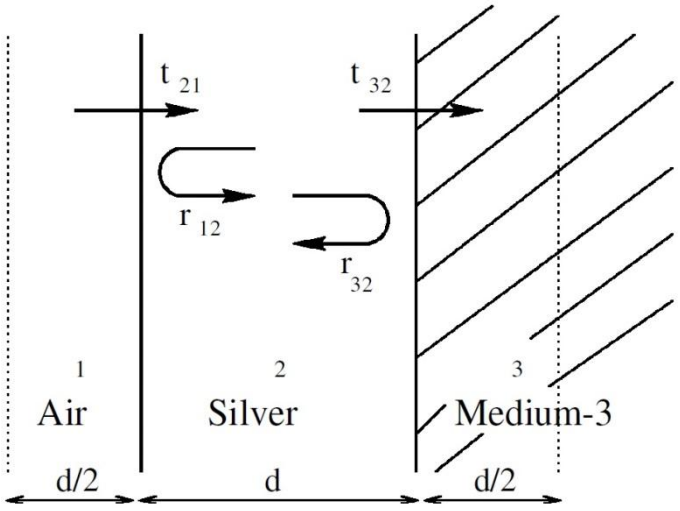

Figure 4.6 [13]. Geometry of an asymmetric lens system

For the sake of simplicity, the authors consider only one transverse component of the wavevector (namely, k_x) and perform an analysis of transition and reflection coefficients similar to that carried out in Pendry's paper [11]. A conclusion is drawn that, unless the electrostatic or magnetostatic limit is considered, aberrations are unavoidable, and therefore this asymmetric system is called by the authors as "a near-perfect lens".

The electrostatic approximation (that is, $k_x \to \infty$) is further considered. Amplification of evanescent waves is shown to occur if ε_2 is equal to either $-\varepsilon_1$ or $-\varepsilon_3$. The transmission coefficient is shown not to be affected by this choice, whereas the reflection coefficient R is shown to be so:

$$R(\varepsilon_2 = -\varepsilon_1) = \frac{\varepsilon_3 - \varepsilon_1}{\varepsilon_3 + \varepsilon_1} \exp(2dk_x), \quad (4.5a)$$

$$R(\varepsilon_2 = -\varepsilon_3) = \frac{\varepsilon_3 - \varepsilon_1}{\varepsilon_3 + \varepsilon_1}. \quad (4.5b)$$

In the former case, reflection is stronger, and therefore the authors call this case "unfavorable". Their calculations show (see Fig. 4.7) that the field strength increases within the slab in case of the symmetric and favorable asymmetric configuration (and this strength at the image plane might exceed the same value at the object plane) and decreases if $\varepsilon_2 = -\varepsilon_1$.

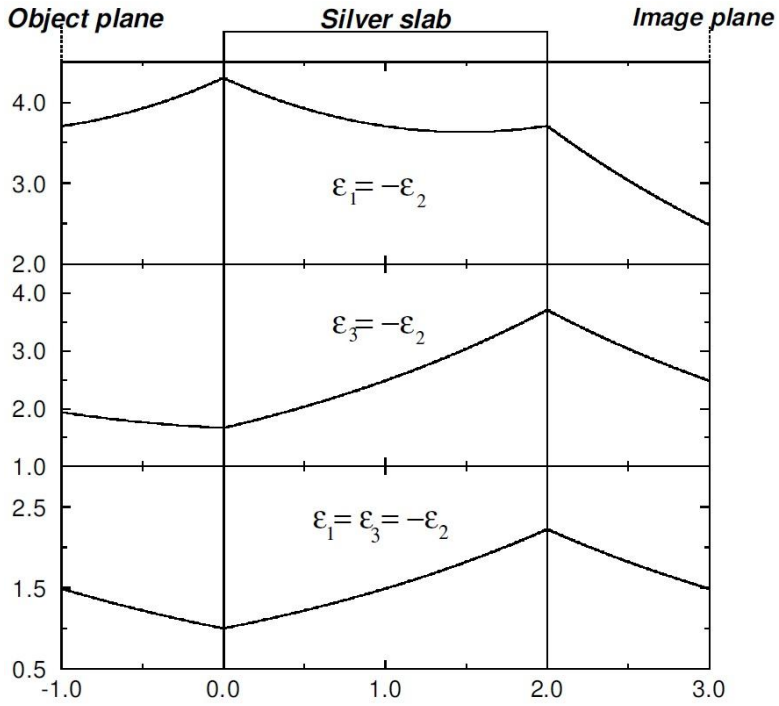

Figure 4.7 [13]. Calculation results for field strength dependence on the *z*-coordinate within and in the vicinity of a silver slab for the symmetric and the both asymmetric configurations described above

It is then demonstrated that, when taking into account a small absorption in the silver slab, that is, presuming $\varepsilon_2 \equiv -\varepsilon_k + i\varepsilon'_2$, where $\varepsilon'_2 << \varepsilon_k$, the configuration $\varepsilon_2 = -\varepsilon_3$ remains "favorable" since the transfer coefficient is higher in this case.

The authors also present the quantitative estimate for the smallest feature which may be resolved using the lens in question:

$$\lambda_{\min} = -\frac{4\pi d}{\ln\left|\frac{\varepsilon_2'}{2\varepsilon_k}\right|}. \qquad (4.6)$$

This confirms the qualitative conclusion drawn by Pendry in [11] that "only the finite imaginary part of the dielectric function prevents ideal reconstruction". On the other hand, the results of the simulations shown in Fig. 4.8 indicate that absorption is "vital for the image formation" as it is emphasized in [13].

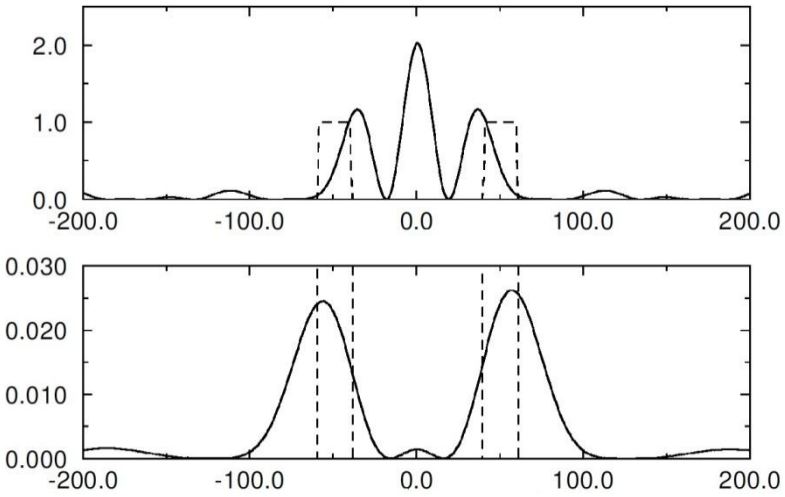

Figure 4.8 [13]. Intensity distribution versus the transverse coordinate in the image plane in case of a symmetric lens. The dashed lines depict the two 20 nm thick slits separated by a distance of 100 nm which are regarded as the object. The thickness of the silver slab surrounded by air from the both sides is 40 nm. Thanks to absorption, the central peak occurring in the upper image (where the slab is presumed to be non-lossy) is absent from the lower one (where the slab is presumed to be lossy).

The “wrong” peak in the center of the upper image is related to the fact that the illumination frequency is always finite, and therefore the electrostatic limit applied in the simulations is, strictly speaking, not applicable. Instead, not only the permittivity values of the slab and the surrounding medium (here - vacuum), but also the permeability values are to be matched (the latter, as said, is not done as the simulations yielding Fig. 4.8 were deliberately carried out in the electrostatic limit).

Pendry’s conception of the perfect lens was later successfully confirmed experimentally. Melville and Blaikie [14] investigated the arrangement with a silver slab schematically shown below.

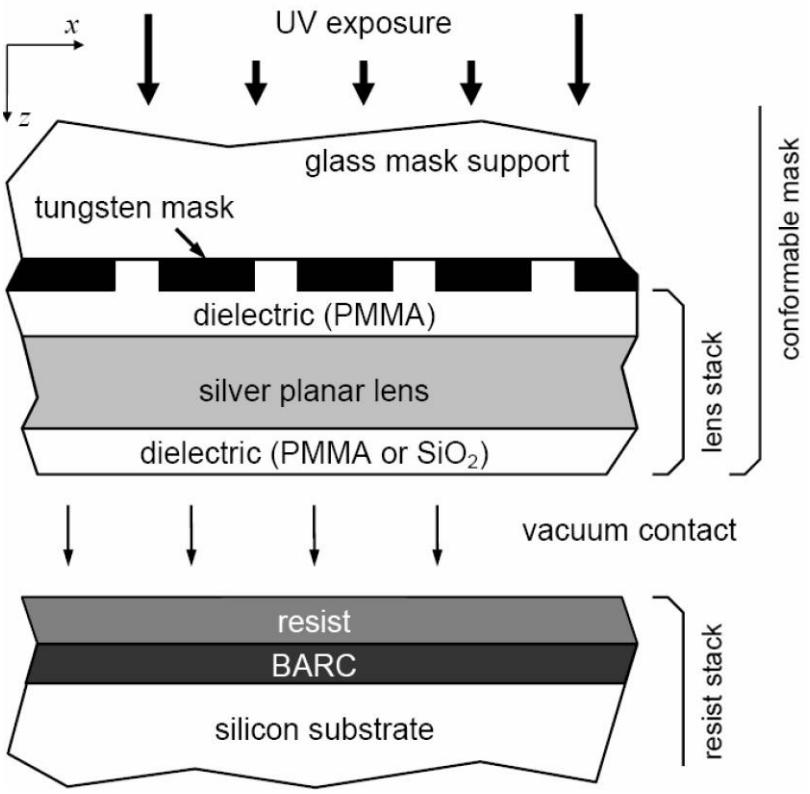

Figure 4.9 [14]. The experimental near field imaging arrangement investigated in [14]. BARC means bottom antireflection coating, PMMA means polymethylmetacrylate

During the experiment, gratings with different periods were illuminated by a wavelength of 365 nm. The lens stack consisted of layers of PMMA, silver and SiO_2 which were 25, 50 and 10 nm thick, correspondingly. As the refractive index of SiO_2 is 1.5, the minimum period which could be resolved was 243 nm due to the far-field limit. However, gratings with the periods of 200 nm and 170 nm were resolved as it is shown below.

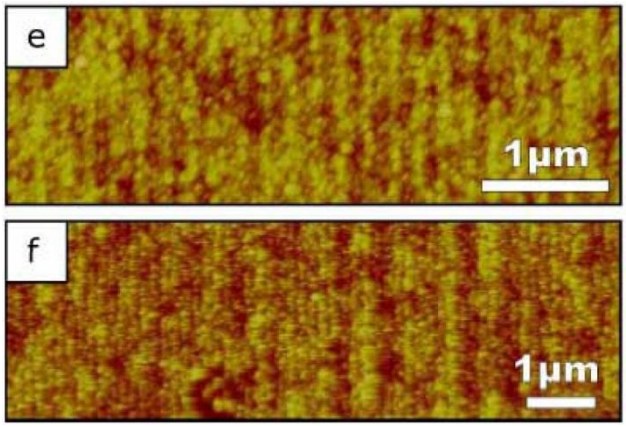

Figure 4.10 [14]. Gratings with periods below the diffraction limit were resolved during the experiment. The images correspond to the 200 nm (the upper image) and 170 nm (the lower image) period gratings

The authors insist that a 145 nm grating was also resolved which follows from the Fourier transform in the direction of the grating vector shown below.

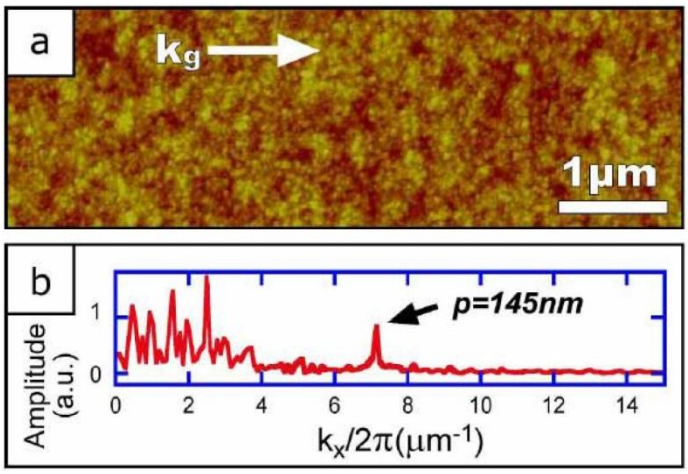

Figure 4.11 [14]. The image of a 145 nm period grating and the Fourier transform of it

Moreover, the authors claim that, according to their calculations, objects with a size lower than 100 nm might be resolved by such a lens system provided the roughness of the films used is reduced (in the setup investigated, the root-mean-square roughness was circa 1 nm).

The report on a resembling experiment carried out by Fang et al. was published just a month later [15]. The arrangement of the experimental setup is shown below.

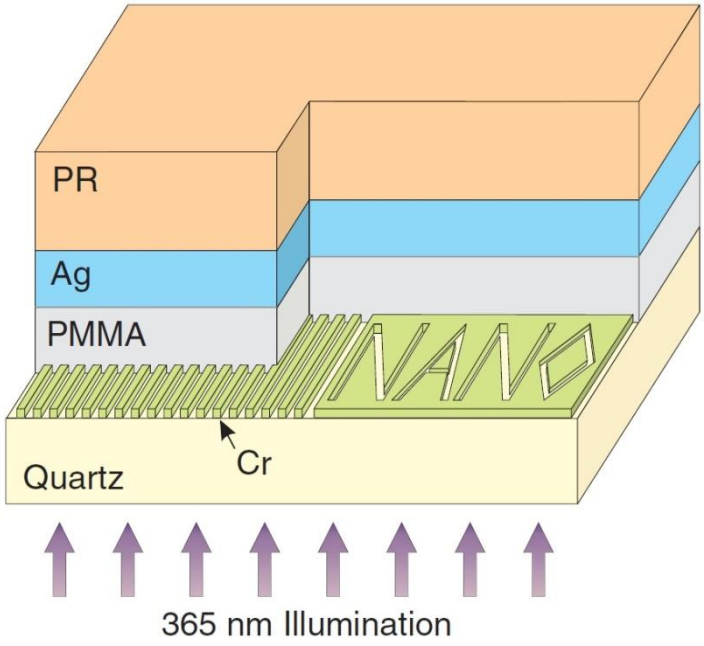

Figure 4.12 [15]. The experimental setup investigated by Fang et al. The thickness of the silver slab is 35 nm, the thickness of the PMMA layer is 40 nm. PR means photoresist

Images of an array of 60 nm wide slots of 120 nm pitch with the silver slab and with an additional PMMA layer substituting the slab are shown below and clearly demonstrate the positive impact of the silver slab on the quality of the image.

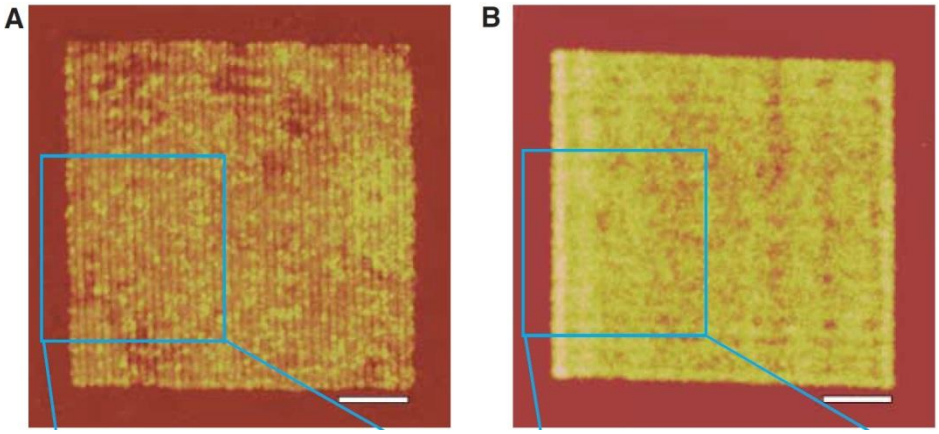

Figure 4.13 [15]. Image of the grating described above in the presence of the silver slab (A) and in the absence of it (B). The scale bar is 1 μm

The advantage of use of the silver slab was also proved for somewhat more sophisticated objects as shown below.

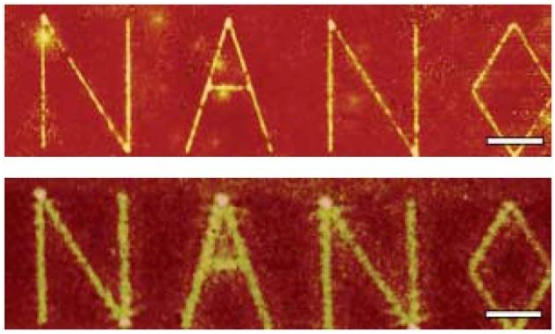

Figure 4.14 [15]. The upper image was obtained with the silver slab, the lower – with a PMMA layer instead of it. The scale bar is 2 μm, the width of the lines is 40 nm

Lastly, it should be noted that, in principle, there is an optimum thickness of the silver slab, for if it is too thick, the absorption prevents the amplification of the evanescent waves. This is clearly confirmed by the calculation results presented in [15].

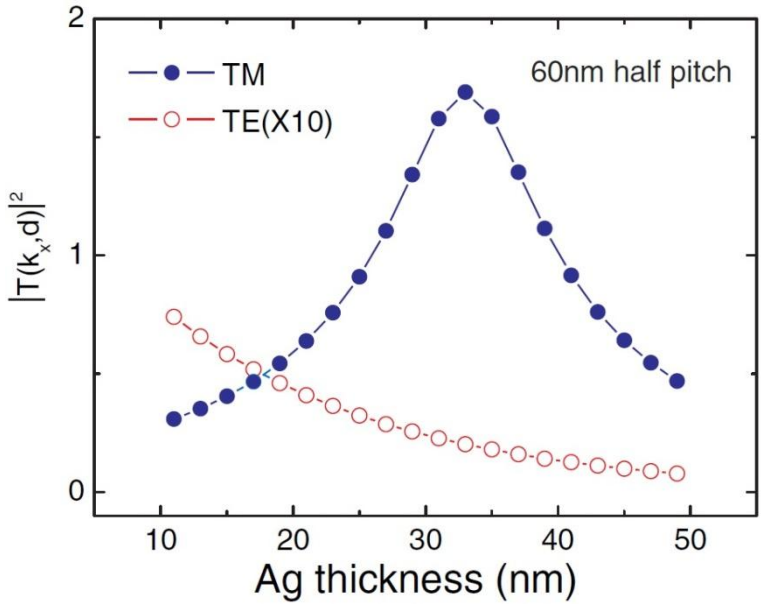

Figure 4.15 [15]. The results of calculations for the image transfer function defined as $|E_{image}|/|E_{object}|$. The object is presumed to have a 60 nm half-pitch

5 CONCLUSIONS

Wave propagation in LHM is a subsection of classical wave physics. However, its history is surprisingly unusual and young. Systematic research in this area started rather recently, in the late 1960s. The cause of this start may neither look very typical, it was namely imagination of a scientist rather than a result of an experiment which would need to be explained.

This area had remained a challenge for scientists during more than 30 years. The reason of this is that NRI-materials are not naturally occurring, but designing such materials turned out to be a rather difficult task. From the practical point of view, it remains a cutting edge also today as it often implies production of and experiments with materials a typical size of which is hundreds and even tens of nanometers. Moreover, even the theory behind such materials is not always agreed upon between scientists. A good example in this regard is the perfect lens. It is enough to say that Veselago was doubtful on its ability to yield focusing below diffraction limit [4].

Thanks to the ideas on practical realization of materials with negative permittivity and permeability proposed by Pendry in the end of 1990s, it became possible to confirm not only such fundamental prediction as refraction of a ray propagating in a LHM at a negative angle, but also his predictions on the perfect lens. However, the experiments with it were carried out presuming the electrostatic approximation, and it would be important to design a perfect lens with both permittivity and permeability negative.

Article [16] outlines a rather brilliant outlook for development and practical use of materials which derive their special properties thanks to the peculiarities of their structure on the subwavelength scale. Namely, the following is said about the NRI-materials: “The “forbidden fruit” of negative-index metamaterial is ripe: the concept is now widely accepted and research is now moving into domain of application”. In addition to the perfect lens, an example of such an application might

be use of LHMs in combination with antennas to enhance their characteristics. In paper [17] by Ziolkowski and Kipple, an idealized arrangement consisting of a small electric dipole surrounded by a shell of a non-lossy isotropic LHM is considered.

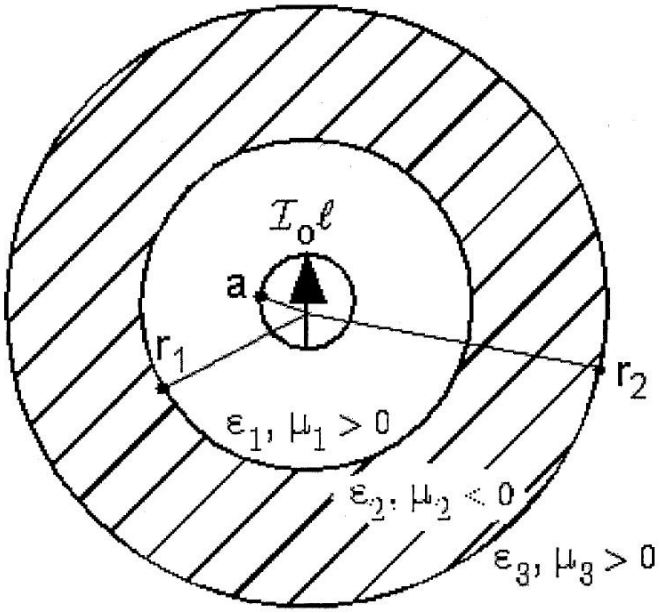

Figure 5.1 [17]. An infinitesimal electric dipole with a length of *l* placed in RHM 1 and separated from RHM 3 by LHM 2

Namely, the radiated and the reactive power which correspondingly are the real and the imaginary part of the complex power *P* flowing through the surface *S* of the imagined sphere with a radius of $a = l/2$ surrounding the dipole are taken up:

$$P = \frac{1}{2}\oiint_S \left[\overrightarrow{E_\omega}\ \overrightarrow{H_\omega^*}\right]\vec{r}\,dS = P_{\text{rad}} + iP_{\text{reac}}, \qquad (5.1)$$

where ***r*** is the unit normal pointed into the volume outside of the sphere *S*. Using the expressions for the components of the TM-field irradiated by the dipole and presuming that the both RHMs are vacuum, $\varepsilon_2 = \mu_2 = -1$, $f = 10$ GHz, $I_0 = 1$ A, $l = 0.06$ μm, $r_1 = 100$ μm, the radiated power gain defined as $P_{\text{gain}} \equiv P_{\text{rad, LHM}} / P_{\text{rad, RHM}}$ was calculated as a function of r_2 for $r_2 \geq r_1$. The resulting curve presented in Fig. 5.2 clearly indicates that use of a shell of an LHM might significantly enhance the properties of an antenna.

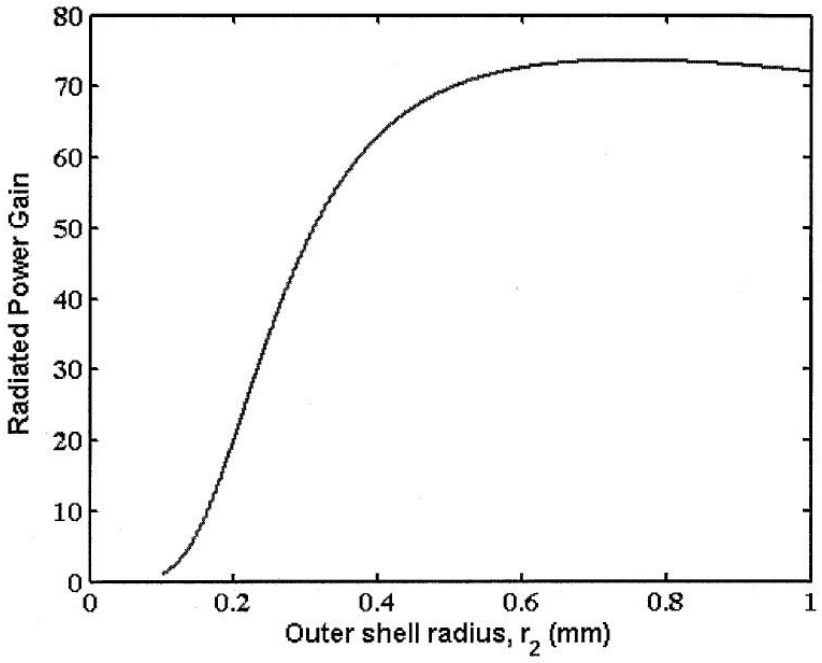

Figure 5.2 [17]. The radiated power gain of a dipole surrounded by a shell made of an LHM with n = -1 versus the outer radius of the shell. The maximum value of the gain for the values of the parameters of the problem described above takes place at r_2 = 748.8 μm

Obviously, such a striking result may have a great practical importance. However, this work received merciless criticism in [18] where it was, by the way, stated: "The results of the commented paper are of no value for evaluating the performance of small antennas surrounded by double negative material". Thus, here we see another example of disagreement between scientists on theoretical predictions made for LHMs. Although Ziolkowski tried to defend paper [17] in his reply [19], the best answer would be an experimental setup confirming the advantages of use of LHMs in combination with antennas. Actually, this can be said about the whole area of LHMs, and one might therefore expect that the academic community engaged in this area will in close future put the most of its efforts in designing new examples of such materials, practically verifying their thrilling properties predicted by the theory and, in the best case, even starting to propose useful applications underlain by these properties.

REFERENCES

1. Veselago, V. G. 1967. Electrodynamics of substances with simultaneously negative electrical and magnetic permeabilities. *Usp. Fiz. Nauk* **92**, 517-526 (*in Russian*)
2. Shalaev, V. M. 2007. Optical negative-index metamaterials. *Nature photonics* **1**, 41-48
3. Pendry, J. B. 2004. Negative Refraction. *Contemporary Physics* **45**, 191-202
4. Veselago, V. G. 2003. Electrodynamics of materials with negative refractive index. *Usp. Fiz. Nauk* **173**, 790-794 (*in Russian*)
5. Pendry, J. B. 1996. Extremely Low Frequency Plasmons in Metallic Mesostructures. *Physical Review Letters* **76**, 4773-4776
6. Pendry, J. B. 1999. Magnetism from Conductors and Enhanced Nonlinear Phenomena. *IEEE Transactions on Microwave Theory and Techniques* **47**, 2075-2084
7. Smith, D. R., Padilla, W. J., Vier, D. C., Nemat-Nasser, S. C. & Schultz, S. 2000. Composite Medium with Simultaneously Negative Permeability and Permittivity. *Physical Review Letters* **84**, 4184-4187
8. Shalaev, V. M., Cai, W., Chettiar, U. K., Yuan, H.-K., Sarychev, A. K., Drachev, V. P. & Kildishev, A. V. 2005. Negative index of refraction in optical metamaterials. *Optics Letters* **30,** 3356-3358
9. Shelby, R. A., Smith, D. R., & Schultz, S. 2001. Experimental Verification of a Negative Index of Refraction. *Science* **292**, 77-79
10. Lee, S. H., Park, C. M., Seo, Y. M. & Kim, C. K. 2010. Reversed Doppler effect in double negative metamaterials. *Physical Review B* **81**, 241102(1-4)
11. Pendry, J. B. 2000. Negative Refraction Makes a Perfect Lens. *Physical Review Letters* **85**, 3966-3969
12. Peiponen, K.-E., Lucarini, V., Vartiainen, E. M. & Saarinen, J. J. 2004. Kramers-Kronig relations and sum rules of negative refractive index media. *Eur. Phys. J. B* **41**, 61-65

13. Ramakrishna, S. A., Pendry, J. B., Schurig, D., Smith, D. R. & Schultz, S. 2002. The asymmetric lossy near-perfect lens. *Journal of Modern Optics* **41**, 1747-1762
14. Melville, D. O. S & Blaikie, R. J. 2005. Super-resolution imaging through a planar silver layer. *Optics Express* **13**, 2127-2134
15. Fang, N., Lee, H., Sun, C. & Zhang, X. 2005. Sub–Diffraction-Limited Optical Imaging with a Silver Superlens. *Science* **308**, 534-537
16. Zheludev, N. I. 2010. The Road Ahead for Metamaterials. *Science* **328**, 582-583
17. Ziolkowski, R. W. & Kipple, A. D. 2003. Application of Double Negative Materials to Increase the Power Radiated by Electrically Small Antennas. *IEEE Transactions on Antennas and Propagation* **51**, 2626-2640
18. Kildal, P.-S. 2006. Comments on "Application of Double Negative Materials to Increase the Power Radiated by Electrically Small Antennas". *IEEE Transactions on Antennas and Propagation* **54**, 766
19. Ziolkowski, R. W. 2006. Reply to 'Comments on "Application of Double Negative Materials to Increase the Power Radiated by Electrically Small Antennas"'. *IEEE Transactions on Antennas and Propagation* **54**, 766-767